Control algorithm for the petal-shape segmented-mirror telescope with 18 mirrors

Atsushi Shimono[a], Fumihide Iwamuro[b], Mikio Kurita[b], Yuki Moritani[b,c], Masaru Kino[d], Toshinori Maihara[e], Hideyuki Izumiura[f], and Michitoshi Yoshida[c]

[a]IPMU, Univ. of Tokyo, Kashiwanoha, Kashiwa, Japan;
[b]Department of Astronomy, Kyoto University, Kitashirakawa, Kyoto, Japan;
[c] Hiroshima Astrophysical Science Center, Hiroshima University, Kagamiyama, Higashihiroshima, Japan
[d]Graduate School of Science, Nagoya University, Furo-cho, Nagoya, Japan
[e]Nano-Optonics Energy Inc., Nishigotanda, Shinagawa, Japan
[f]Okayama Astrophysical Observatory, NAOJ, Kamogata-cho, Asakuchi-shi, Okayama, Japan

ABSTRACT

A 3.8 m segmented telescope is planned to be built at the Okayama Astrophysical Observatory by the joint program among Kyoto university, Nagoya university, NAOJ, and Nano-Optonics Energy Inc. This is the world's first optical-infrared telescope whose primary mirror is composed of "petal-shaped" segment mirrors.

To investigate the best layout of the displacement sensors as well as to study the control algorithm, we have developed a simulation software for the segmented petaloid mirrors. This simulator calculates the vertical position differences between the segments at the 60 displacement sensors based on the three-dimensional movements of the 54 actuators, and enables us to test the control algorithms under various conditions including random noise on the displacement sensors, random movement errors of the actuators, and unexpected lateral shifts of the segments. The outputs of the simulator are not only the phase error of the primary mirror but also the PSF image, taking the structure function of the optical surfaces into account.

Using a singular value decomposition method, we found that the 18 petal-shaped segments are controllable within the required displacement errors of 15nm under the following three conditions: 1) the displacement measurement sensors are placed in staggered fashion between segments, 2) the displacement measurement sensors are axisymmetrically placed with respect to the optical axis, and 3) the relative lateral shift and rotation of each segment are less than 500 μm and 0.05 degree, respectively.

In this report, the control algorithm, requirements for the layout of the displacement measurement sensors, and the simulated performance will be presented.

Keywords: segmented-mirror telescope, petal-shaped

1. INTRODUCTION

The segmented-mirror telescopes including Keck I and II have been constructed in these 20 years, expanding the frontier of the observational astronomy. All these segmented-mirror telescopes are composed of hexagonal-shaped segments, which are compatible with the truss structure useful for the lightweight mirror-cell. From a viewpoint of the shape of the segments, petal-shaped segments were often compared with the hexagonal-shaped segments. The petal-shaped segments have advantages in the smaller number of the surface-shape as well as in the smooth shape of the point spread function (PSF) through the total aperture, while disadvantages are expected in combination with the truss structure and in measurement of the total shape of the mirror by displacement-measurement sensors (edge sensors) especially for large telescopes.[1] Although it is unknown that

Further author information: (Send correspondence to A.S.)
A.S.: E-mail: atsushi.shimono@ipmu.jp, Telephone: +81 4 7136 5976

Figure 1. The lightweight truss mount assembled in the test room (left). The prototype of the mirror control system attached to the truss mount (right).

Figure 2. Whole view of the machine compared with a human (left). A snapshot taken during a grinding operation (right).

which advantage or disadvantage is the most important factor for a large telescope, the disadvantage is expected to be small when the number of the segments is not so large.

On the other hand, the need for economical medium-aperture telescopes has been increased in recent years, to make a specific observation such as large area surveys. Segmented-mirror telescopes have a possibility not only for the large aperture telescope but for such an economical medium-aperture telescope, if we can make off-axis mirrors by economical manner.

On the basis of these backgrounds, a 3.8 m segmented-mirror telescope is planned to be built at the Okayama Astrophysical Observatory by the joint program among Kyoto university, Nagoya university, NAOJ, and Nano-Optonics Energy Inc. This is the world's first optical-infrared segmented-mirror telescope with 18 petal-shaped segments, having a lightweight truss mount optimized by a genetic-algorithm method.[2] A prototype of the mirror control system has been attached to the truss mount and their basic motion has been tested under the tracking condition of the telescope (Fig. 1). Nano-Optonics Energy has a production capacity of economical segment-mirrors by an ultraprecision grinding and polishing technique (Fig. 2). The surface shape of the polished segment is measured by an interferometer equipping a computer generated hologram (CGH) mask[3] located at 10m above the grinding machine.

In this paper, we demonstrate the control algorithm, requirements for the layout of the edge sensors, and the expected performance of the telescope evaluated by the simulation software for the segmented petaloid mirrors.

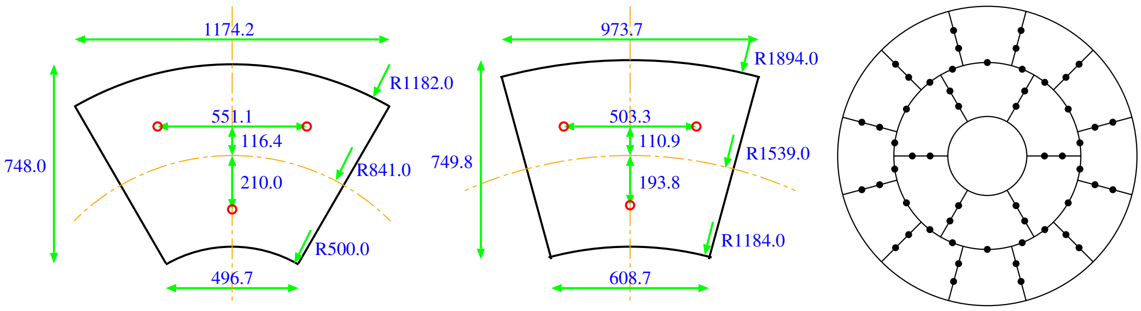

Figure 3. The shapes of the inner/outer segments together with the position of the actuator (left). The layout of the segments marked with rough positions of the edge sensors (right).

2. SIMULATION SOFTWARE

To estimate the expected performance of the segmented petaloid mirrors, we developed a simulation software optimized for the 3.8m telescope. In this section, we represent the specification in detail.

2.1 Components

Although a lot of components required to control the segmented-mirror, only the mechanical edge sensors and the segmented mirrors with three actuators for each (Fig. 3) are included in this simulator to simplify the goal: 1) determine the most effective layout of the edge sensors, 2) estimate the tolerance for lateral shifts of the segments, and 3) evaluate the propagation effects of the sensor noise on the total shape of the mirror. The Shack-Hartmann camera and the phase-camera system are not taken into account here.

The 3.8m telescope has 18 (inner 6 and outer 12) segments with 54 actuators. To determine the position of these actuators, at least 54 edge sensors are required. The most reasonable layout of the edge sensors of this number is shown in Fig. 3; 12 sensors along the inner radial edge, 24 along the outer radial edge, and the remaining 18 along the circumference between the inner and the outer segments. Obviously three degrees of freedom (parallel axial shift and tilts) cannot be fixed by this layout. (In a strict sense, the segments cannot be moved with a constant separation because the actuators are not parallel between the segments, see Fig. 4.) We neglect these three degrees of freedom here because these components are easily fixed by extra three sensors or keeping three actuators at fixed position. Thus the input conditions are the 54 values of the edge sensors and the output values are the travel distances of 54 actuators with 51 degrees of freedom to be fixed.

2.2 Algorithm

As explained in the previous subsection, we can define the actuator vector X and the sensor vector Y as 54-dimensional vectors. The conversion matrix A defined by

$$Y = AX \tag{1}$$

is determined for the given relative position of sensors to each segment, because the ideal positions of the segments are predetermined. Here, the structure of the edge sensor is defined by a point (the center of the sensing aperture) and a plane (the target plate) which has the same normal vector of the mirror surface right above the position of the sensor (see Fig. 4).

In fact, the conversion matrix A is measured through the constant movement of the actuators one by one. As a result, A has only 5-7 non-zero components along the columns depend on the number of the sensors attached to a segment. The measured matrix A' is affected by the noise of the sensors, which is evaluated in the section 4.

The singular values and the corresponding orthonormal basis of the conversion matrix A is calculated using the singular value decomposition (SVD) method in the GNU Scientific Library *. Since the distribution of the singular values are depend on the layout of the edge sensors, the best layout is determined to make the minimum

*http://www.gnu.org/software/gsl/manual/html_node/Singular-Value-Decomposition.html

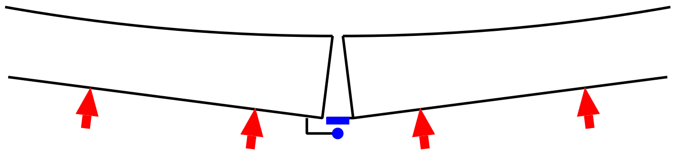

Figure 4. A edge sensor is defined by a point and a plane whose normal vector has the same direction of the mirror surface right above the position of the sensor. The output value of the sensor is the gap between the point and the plane. Arrows indicate the actuators.

singular value as large as possible. One of the actuator vector X is calculated from the sensor vector Y using the pseudo-inverse matrix A^+ with ignoring singular vectors which have smaller singular value than threshold defined by control parameter.

$$X = A^+ Y; \tag{2}$$

Note that the actuator vector X obtained by equation 2 includes irrelevant parallel shift and tilts, which are removed to make the mean residual error of the wavefront zero. The false output of the sensor caused by the noise transfered to the phasing error of the segments through this matrix A^+.

To simulate the point spread function (PSF) of the telescope based on the real data, the structure function of the produced mirror can be incorporated in this simulator. The PSF is generated from the simulated wavefront including the phasing error of the segments.

2.3 Evaluate function

The performance of the conversion matrix is quantified by the minimum singular value except for the unconstrained three modes, parallel shift and tilts. Since smaller singular values mean that the corresponding mode is difficult to control, larger minimum value is required to achieve the stable control of the segments. After optimization of the layout of the edge sensor, the evaluation value of the degree of phasing is needed.

The targeted specification of the telescope optics is the diffraction limit in the H-band ($\lambda = 1.65\mu$m), i.e. 100 milliarcsec (mas) or the maximum phasing error of the segment less than 200nm. Although the phasing performance should be evaluated by the FWHM of the PSF, it is difficult to determine if the PSF has an abnormal shape such as multi cores or very broad wing. Thus we define the pseudo-FWHM from the Strehl ratio of the PSF, which is the expected FWHM of the Gaussian PSF having the measured Strehl ratio. In the next section, we show the results of the optimization of the layout of the edge sensor as well as the expected phasing performance using this evaluation value.

3. RESULTS

Fig. 5 shows the singular vectors sorted in descending order of the singular values. This result indicates that the simple layout of the edge sensors in Fig. 3 has four modes difficult to control (#48-51 in Fig. 5). These modes have very small singular values less than 1% of the maximum value (mode #1). This tendency does not change if we move any sensors along the edge of the segments. We tried various layout pattern and found that the most effective one is the axisymmetric-staggered layout along radial direction (open symbols in Fig. 6). We also found that the additional 6 sensors attached to the single ring structure along the inner edge of the inner segments increase the minimum singular value by half. In this case, we add three more virtual actuators to support the inner ring structure; total 60 edge sensors and 57 actuators with 54 degrees of freedom to be fixed.

The singular vectors of the actuators for this axisymmetric-staggered layout of the sensors are shown in Fig. 7. The four modes having very small singular vectors in Fig. 5 become controllable (#51-54 in Fig. 7). Although longer arms of the displaced sensors make the minimum singular value larger, they may cause another problem on stability of the relative position between the segment and the attached sensors. Farther investigation using the real structure is required to determine the most effective arm length of the displaced sensors.

For the axisymmetric-staggered layout of the edge sensor (Fig. 6), we simulated the phase control of the segments under the uniform sensor noise between ±15nm. As expected from the singular values, two folding

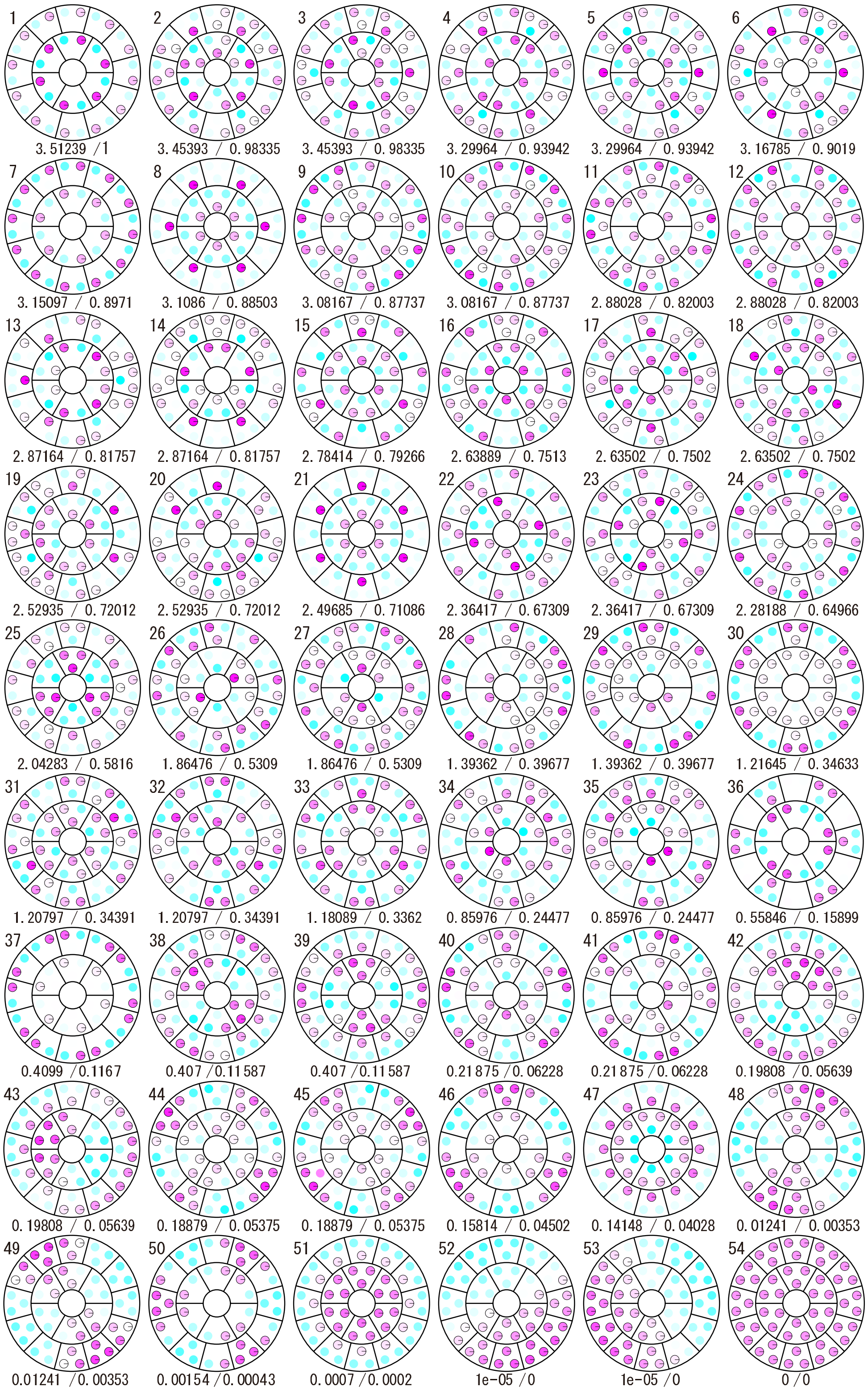

Figure 5. The singular vectors of the actuators sorted in descending order of the singular values are presented. Each singular value is shown at the bottom of the corresponding mode together with the normalized one by the maximum singular value. Circled (non-circled) points indicate the plus (minus) direction movement of the actuator.

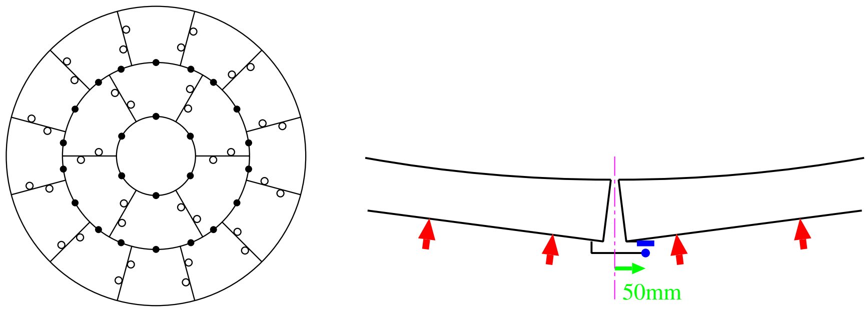

Figure 6. The open circles indicate the edge sensors with orthogonal offset of 50mm to the edge of the segments (left). The definition of the sensor in the simulator is the same as that of shown in Fig. 4 except for the long arm of the sensor (right).

modes (#53 and #54 in Fig. 7) and the curvature changing mode (#52) often appeared in the feedback commands to the actuators. However, the distribution of the feedback amount to the actuators is not so large compared with that of the edge sensors, less than ∼25nm after the parallel shift and tilts components are subtracted.

The effects of lateral shifts and rotation of the segments as well as the effect of the production error of the curvature radius among segments (designed value of 10m) are defined as the level increasing the pseudo-FWHM of the PSF by 100mas. Table 1 and Table 2 shows the increased amount of the pseudo-FWHM under various conditions. From the results of these calculations, the errors contributing 100mas increase of the pseudo-FWHM are as follows.

- ∼75nm error of the actuator
- $\sim \pm 100\mu$m error of the curvature radius
- ∼0.07 degree rotation of the segment
- < 1mm shifts of the segment is allowed

The lateral shift of the segment is almost canceled by the movement of the actuator naturally, because the target plate of the sensor is parallel to the surface of the mirror. The relative position between one segment and a part of the neighbor mirror surface right above the position of the target plate is maintained if the separation between the segments is changed slightly. In the next section, we discuss the expected operation sequence from these results.

4. DISCUSSION

As mentioned in section 2.2, the conversion matrix A has to be determined by constant reciprocating motion of each actuator. We found that 20μm stroke is enough to suppress the contribution of the typical sensor noise of 15nm, if the nonlinear characteristics of the sensors are completely corrected. For longer stroke than 20μm, the singular values and the corresponding pattern of the singular vectors of the measured conversion matrix A' are almost constant.

During the feedback operation to maintain the total figure of the mirror, different sets of the feedback parameters should be applied to different modes. For example, unstable modes with smaller singular values should be controlled with a larger contribution of the integral term to stabilize them. This mode-separated control will be investigated further in the future.

Taking the structure function of the mirror surface into account, the lateral shifts, rotations, and the phasing error of each mirror should be less than ∼500 μm, 0.05 degree, and 50nm, respectively, to keep the pseudo-FWHM of the PSF ∼200 mas, assuming the production error of the curvature radius is less than $\sim 50\mu$m. All

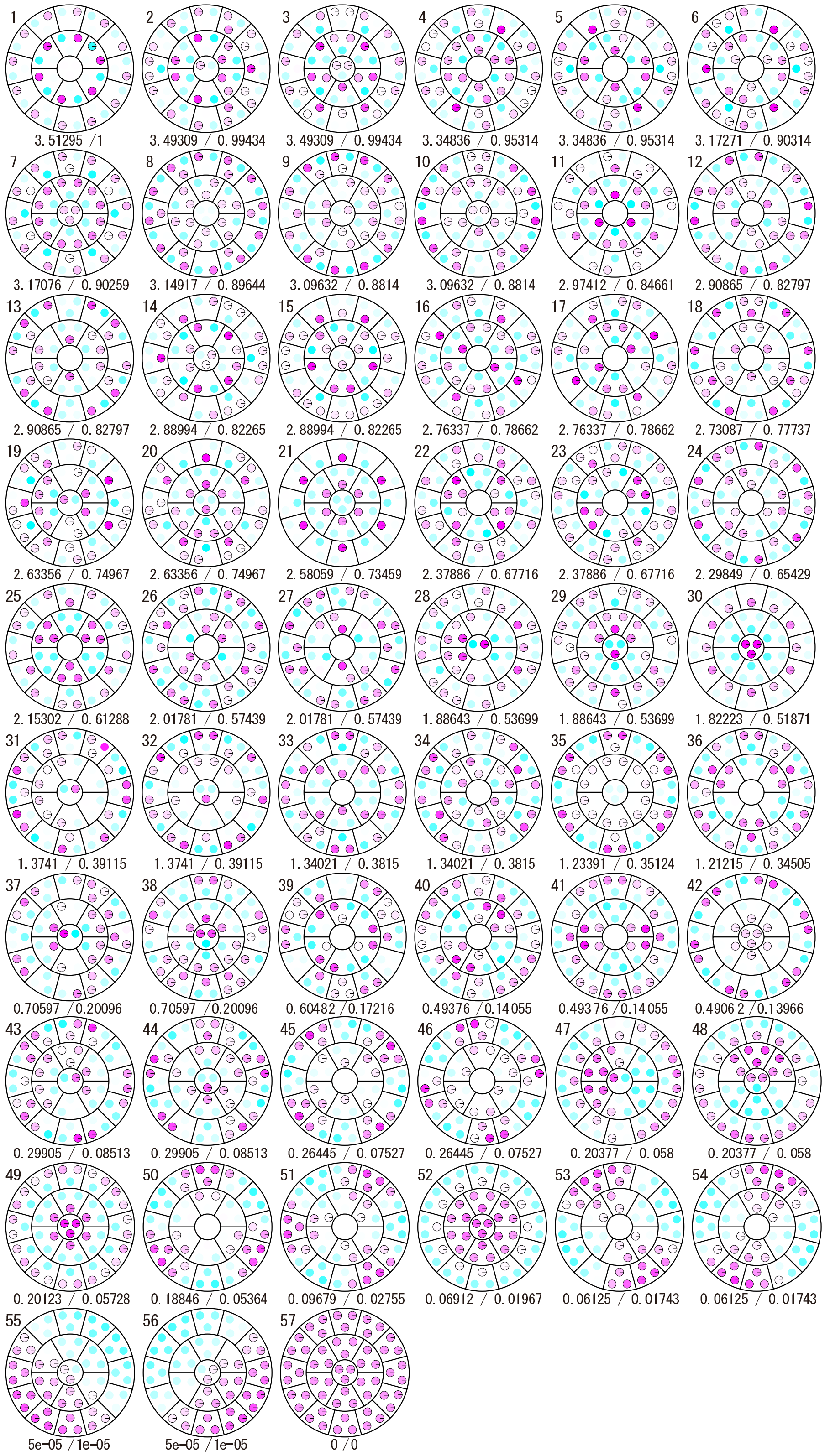

Figure 7. The layout of the sensors corresponding these singular vectors is presented in Fig. 6. The minimum singular value except for parallel shift and tilts modes is about 1.7% of the maximum value.

Table 1. Increased amount of the pseudo-FWHM of the PSF in milliarcsec (mas). Zero means the ideal diffraction pattern of the PSF of 110mas. The structure function of the surface of the segment is comparable with that of the atmospheric turbulence with Fried parameter of $r_0 = 92$cm.

No atmospheric turbulence

	Error of the curvature radius			
Phasing error	0μm	$\pm 50\mu$m	$\pm 100\mu$m	$\pm 200\mu$m
0nm	0	40	83	258
$\pm$50nm	54	68	105	288
$\pm$100nm	118	131	169	397

Under atmospheric turbulence of $r_0 = 92$cm

	Error of the curvature radius			
Phasing error	0μm	$\pm 50\mu$m	$\pm 100\mu$m	$\pm 200\mu$m
0nm	41	59	100	283
$\pm$50nm	63	78	116	310
$\pm$100nm	124	138	179	418

Table 2. Effects of lateral shifts and rotation of the segments on the pseudo-FWHM of the PSF. Increased amount of the pseudo-FWHM are listed in the same manner of Table 1. X, Y, and θ correspond to tangential, radial, and rotational movement of the segment, respectively. The unit of column #1 is mm for X and Y, or degree for θ.

Variation [mm or °]	X	Y	θ
0.01	6.4	12.3	20.2
0.05	6.4	15.4	63.4
0.1	13.6	21.3	133.9
0.5	22.8	33.6	2439

these requirements are confirmed to be almost accomplished though the test using the actual telescope mount shown in Fig. 1.

The source code of this simulator is written with an aim to control the real telescope after the control modules of the actuators and the sensors are linked with the source. This is the most reliable way to control the complicated structure such as segmented mirrors.

REFERENCES

[1] Strom, S. E., Stepp, L. M., and Gregory, B., "Giant segmented mirror telescope: a point design based on science drivers," in [*Society of Photo-Optical Instrumentation Engineers (SPIE) Conference Series*], Angel, J. R. P. and Gilmozzi, R., eds., *Society of Photo-Optical Instrumentation Engineers (SPIE) Conference Series* **4840**, 116–128 (Jan. 2003).

[2] Kurita, M., Ohmori, H., Kunda, M., Kawamura, H., Noda, N., Seki, T., Nishimura, Y., Yoshida, M., Sato, S., and Nagata, T., "Light-weight telescope structure optimized by genetic algorithm," in [*Society of Photo-Optical Instrumentation Engineers (SPIE) Conference Series*], *Society of Photo-Optical Instrumentation Engineers (SPIE) Conference Series* **7733** (July 2010).

[3] Kino, M., Kurita, M., and Sato, S., "Interferometric testing for off-axis aspherical mirrors with computer-generated holograms," *Applied Optics* (in press, 2012).